DNA Nanostructures

DOI: 10.1002/anie.201202816

Design Strategy for DNA Rotaxanes with a Mechanically Reinforced PX100 Axle**

*Damian Ackermann, Stefan-S. Jester, and Michael Famulok**

Rotaxanes are interlocked molecular architectures that can be perceived as simple mechanical devices.[1] A macrocycle that is threaded onto an axle and is deterred from dethreading by bulky stoppers can move translationally along the vector of the axle as well as rotate around it. To ensure that these molecular assemblies can carry out directional mechanical motion, the respective components require sufficient dimensional stability, or stiffness, over the entire working space.[2] In case of rotaxanes, it is primarily the axle that needs to exist as a non-deformable unit to efficiently convert the microscopic movement of the macrocycle into mechanical energy and to employ it for power transmission, otherwise the momentum of the moving macrocycle simply leads to a deformation of the axle, and thus cannot be further employed. We have recently described a DNA rotaxane that has a translational amplitude of about 100 base pairs (bp).[3] In a double-stranded DNA, however, the length of persistence of approximately 130 bp is too short to meet the required mechanical stability along the dumbbell axle.[4]

Many systematic studies have devised methods in structural DNA nanotechnology[5] that not only allow for the construction of topologically defined architectures by self-assembly of DNA sequences, but also lead to robust two- and three-dimensional objects.[6] Seminal work in this field was established by Seeman, who demonstrated that two DNA double strands that are interwoven by multiple reciprocal strand exchange can lead to molecular assemblies that exhibit increased stiffness.[4,7] Among them, particularly the so-called paranemic crossover structures PX and JX[8] were often applied for mechanical switching in DNA nanotechnology.[9] PX elements are characterized by a strand exchange that occurs at each contact point of two antiparallel DNA double strands. In a JX element, however, the strand exchange is abrogated at two consecutive positions. What makes the PX and JX elements so special is that two independent DNA double strands can be held together by reciprocal base pairing. Consequently, a paranemic crossover structure always exists in equilibrium with the respective DNA double strands. In presence of Mg^{2+} ions, the equilibrium is strongly shifted towards the crossover product.[10]

For the assembly of dsDNA rotaxanes, we devised a threading strategy that relies on the formation of eight bp between the DNA axle and the macrocycle.[3] The hybridization of these two components occurs highly efficiently, leading to quantitative rotaxane formation. Owing to the highly flexible single-stranded region, the DNA axle is able to easily accommodate its conformation to the geometry inherent to the macrocycle, thus leading to quantitative threading of the axle. However, higher-order DNA architectures like paranemic crossover DNA or even DNA origami[11,12] do not permit this flexibility anymore. On the contrary: it is precisely their mechanical robustness that accounts for their importance in DNA nanotechnology. Conversely, however, this lack of flexibility constitutes a major challenge for the threading of a rotaxane axle into a macrocycle that necessitates novel design strategies, which we describe herein.

To expand the range of application of mechanically interlocked DNA architectures to these higher-order DNA structures, we sought to apply our threading strategy to a robust paranemic crossover system and to assemble the PX100 rotaxane (Figure 1a). The reinforcement of the dumbbell axle is achieved by an extended PX-JX2 crossover system in which two parallel DNA double strands are interwoven by six double crossovers (Figure 1b). A pivotal

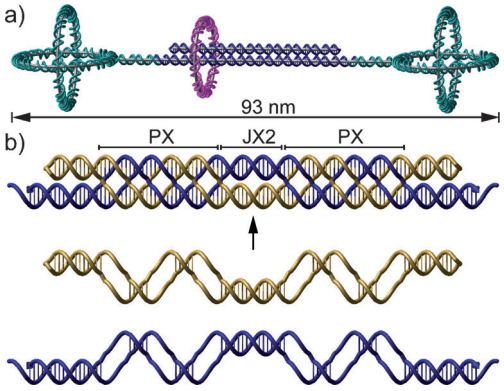

Figure 1. Paranemic crossovers in a PX100-DNA rotaxane. a) Idealized three-dimensional illustration of the DNA rotaxane with reinforced PX100 axle (blue), spherical stoppers (green), and a fully mobile macrocycle (magenta). b) The PX100 axle is formed by a paranemic strand exchange between a 100-mer DNA dumbbell (gold) and a 113-mer DNA-duplex (blue) containing 5′-overhangs. The images were generated using NANOENGINEER.

[*] Dr. D. Ackermann, Prof. M. Famulok
Universität Bonn, LIMES Institut, Chemical Biology & Med. Chem. Unit c/o Kekulé-Institut für Organische Chemie und Biochemie
Gerhard-Domagk-Strasse 1, 53121 Bonn (Germany)
E-mail: m.famulok@uni-bonn.de
Homepage: http://www.famuloklab.de
Dr. S.-S. Jester
Universität Bonn
Kekulé-Institut für Organische Chemie und Biochemie
Gerhard-Domagk-Strasse 1, 53121 Bonn (Germany)

[**] This work was supported by the European Research Council (ERC Advanced grant No. 267173). We thank H. Haschke, JPK Instruments, for carrying out HyperDrive AFM measurements.

Supporting information for this article is available on the WWW under http://dx.doi.org/10.1002/anie.201202816.

detail in the design of the axle is a section in which two possible crossovers remain unrealized, corresponding to a JX2 element. This section was incorporated into the PX100 element to introduce a single-stranded gap that allows the hybridization with the macrocycle during rotaxane assembly.

Compared to a classical DNA double strand, the gap regions in the PX100 axle as well as in the macrocycle require an entirely different conceptual design. We reasoned that the hybridization over eight nucleobases has to occur at a single continuous DNA strand without including a crossover. Of particular importance is the location of the Watson–Crick sides of all of the nucleobases that participate in the hybridization in an outward position. Only in this case are both partners able to find each other during the bimolecular threading process to form a stable pseudorotaxane. Correspondingly, the DNA sequences were designed so as to ensure hybridization of the two DNA double strands in a 6:5 PX pattern. Energy minimizations as well as the potential pairing patterns were controlled by means of MFOLD (Supporting Information, Figure S1). The complete sequence of the entire PX100 axle is shown in Figure 2a. The selection of the gap region within the JX2 section was derived from a 3D description that is representative for a PX100 axle, generated by means of the NANOENGINEER software (Figure 2b). As can be gathered from Figure 2b, it is possible for the macrocycle to completely align its eight nucleotides designated as the hybridization site with the complementary ss-domain in the PX100 axle by approaching it from an outward position, thereby maximizing the threading efficiency.

The PX100 axle is composed of three DNA sequences. Two of them are 113 nt in size. Together they form the duplex shown in blue that contains sticky ends as 5′-overhangs required for ligating the stopper modules at a later stage of the rotaxane assembly (Figures 1b, 2a). The 191-mer sequence folds into the duplex depicted in brown by forming two hairpin loop structures. Furthermore, this duplex possesses a nine-nt-long single-stranded gap that serves as the hybridization site during the threading of the macrocycle.

The PX100 axle was assembled by slowly cooling the three DNA sequences from 95 °C to 15 °C with a cooling rate of 36 °C h^{-1} in TAE–$MgCl_2$ buffer ("Seeman-buffer"). An almost quantitative formation of the PX100 axle was detectable by polyacrylamide gel electrophoresis (PAGE) (Supporting Information, Figure S2). We purified the PX100 axle by using weak anion-exchange (WAX) HPLC to avoid undesired side-products during rotaxane synthesis. The purified axle is stable for months when stored in Seeman buffer.

In parallel, to maximize the efficiency of threading of the axle into the macrocycle, we optimized the single-stranded region (gap region)[13] of the macrocycle. Thereby, we sought to comply with the NMR structure of an (AT)6-motif, from which it can be deduced that the 5′-A nucleoside within the (AT)6-motif preferentially adopts the outer position in the macrocycle (Figure 2c).[14] Thus, the single-stranded gap in the macrocycle was chosen so as to ensure that the middle of

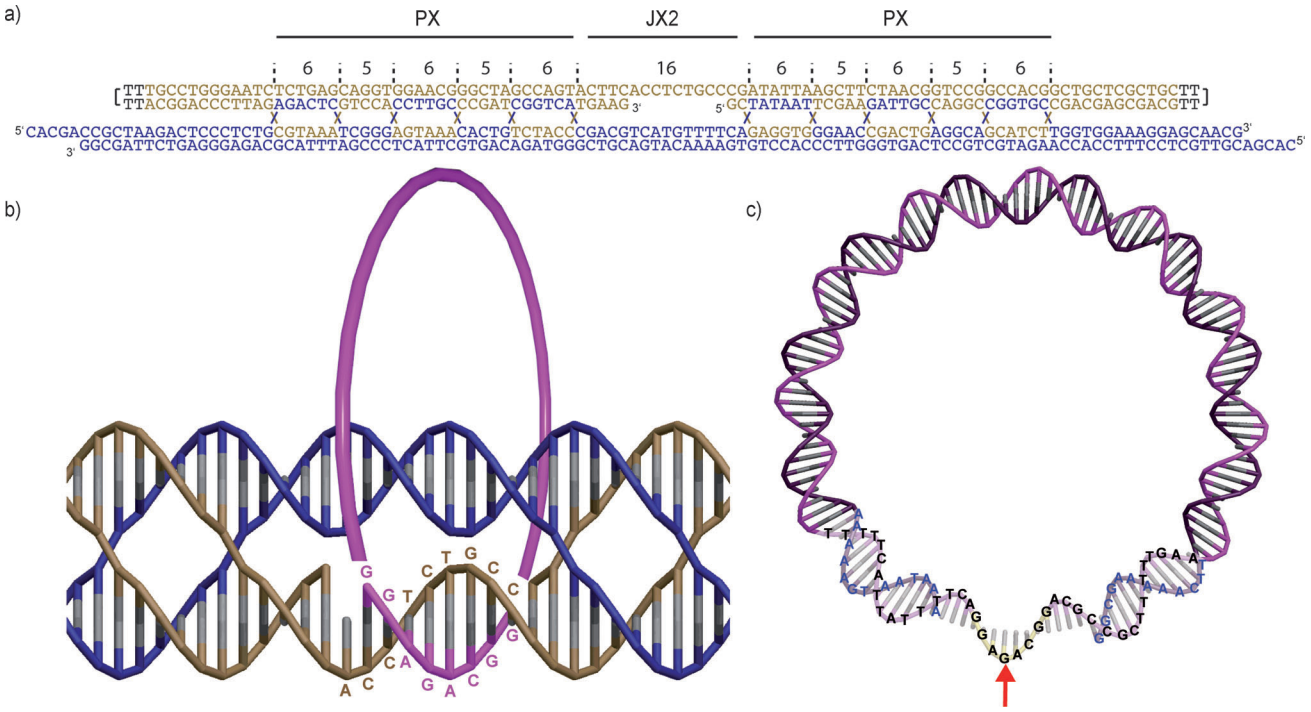

Figure 2. Design of the DNA rotaxane with PX100 axle. a) Structure of the PX100 axle. The DNA sequence constituting the PX100 axle was constructed so as to arrange the components in a 6:5 PX pattern. b) Three-dimensional representation of the PX100 axle harboring the threaded macrocycle. The single-stranded (ss) gap region in the JX2 section was placed so as to ensure that the eight nucleobases that are relevant for threading (CCGTCTCC, gold) are pointing outward. In this way, the macrocycle (magenta) is able to fit snugly onto the axle. c) Three-dimensional representation of the macrocycle PX100GR in its preferred conformation. The site of hybridization with the PX100 axle is located in an outward position in the middle of the gap (G with red arrow) so that the macrocycle can attach to the axle without further reorientation.

the hybridization site also becomes located at an outer position (Figure 2c, red arrow and yellow sequence).

To investigate the threading efficiency, we first assembled pseudorotaxanes in which ordinary 168 bp DNA nanorings were ligated onto the axle to serve as stoppers (Figure 3a). Even though this approach does not generate mechanically stable rotaxanes, these types of rotaxanes have two important

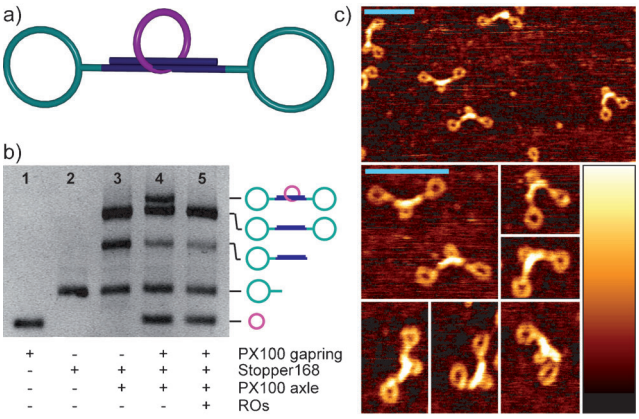

Figure 3. PX100 pseudorotaxane. a) Simplified illustration of the pseudorotaxane containing the ring stoppers (cyan), PX100 axle (blue), and the bound macrocycle (magenta). b) Agarose gel (2.2%) of the pseudorotaxane synthesis. Lane 1: PX100 gap ring; lane 2: 168 bp ring stopper; lane 3: raw product of the dumbbell synthesis; lane 4: raw product of the pseudorotaxane synthesis; lane 5: addition of the two ROs to the pseudorotaxane leads to complete disassembly into the dumbbell and the free macrocycle. c) AFM images of the purified pseudorotaxane. The macrocycle is located in the middle of the axle (scale bar: 100 nm, color coding of height: 0.0–1.0 nm).

advantages. First, the assembly results in a planar architecture that can be readily adsorbed on a mica surface for straightforward characterization by atomic force microscopy (AFM). Second, the addition of a so-called "release oligodeoxynucleotide (RO)" triggers the dethreading of the macrocycle from the dumbbell structure. This can serve as direct evidence for the interlocked nature of the assembly (before the addition of the RO), and for the unhindered movement of the macrocycle after its detachment from the axle.

The pseudorotaxane was assembled in two steps. At first, the macrocycle and the PX100 axle were incubated over night at 12°C, followed by the ligation of the ring stoppers onto both ends of the axle. The ligation was monitored by agarose gel electrophoresis. From the ratio of the bands corresponding to the dumbbell and the rotaxane, respectively, the threading efficiency can be determined. At an overall concentration of 25 mM $MgCl_2$ in 1×ligase buffer at 12°C, the efficiency was around 50% (Supporting Information, Figure S3). Increasing the Mg^{2+} concentration further did not improve the threading. As expected, and as shown in another gel shift experiment, the addition of the two ROs resulted in the detachment of the macrocycle from the axle. Thereby, the pseudorotaxane disassembles into the dumbbell and the free macrocycle by a slippage mechanism (Figure 3b).[15] The interlocked architecture of the pseudorotaxanes that were purified by WAX-HPLC is shown by AFM images (Figure 3c). Special attention should be paid to the PX100 axle, which significantly differs in its diameter and height profile from the ordinary double strands in the ring-stoppers and the macrocycle. Moreover, as expected, the threaded macrocycle is always positioned exactly in the middle of the PX100 axle. The PX100 axle either proceeds completely linear, or exhibits a minimal bending at the binding site of the macrocycle. These observations are in full agreement with our perception of the reinforced axle that can be minimally bent at the JX2 domain in the absence of the RO.

Based on our preceding study, we know that the mechanical blockade of the macrocycle at the dumbbell, and thus the synthesis of a genuine rotaxane, requires the use of spherical stoppers.[3] However, the assembly of the spherical stopper components was hitherto relatively laborious, as it required a three-step synthesis. We therefore improved the assembly of the spherical stoppers in a way that allows obtaining the crossover rings in a two-step procedure that can go without purification of the intermediates.

To this end, the sphere was divided into two rings B and C (Figure 4a). Ring B possesses four overhangs that can bind to the two single-stranded regions of the double-gap ring C. In the first step, these two rings were individually assembled and ligated. When equimolar amounts of ring B and C are combined under ligation conditions, the spherical architecture is generated as a single uniform product (Figure 4b; Supporting Information, Movie 1). After purification by WAX-HPLC, the crossover rings were obtained in sufficient yields of between 10% and 20%.

We have assembled two types of these spherical DNA architectures: the first variant contained a three-way junction at one of the rings that terminated in a sequence complementary to the blue ss overhang of the PX100 axle (Figure 1b) that is subsequently used for ligation of the spherical stoppers. The second variant lacks this bifurcation. In this case we obtained the spherical DNA architecture shown in the right panel of Figure 4b, the spherical crossover structure of which is visualized in excellent resolution in the AFM image (Figure 4c). These entirely spherical DNA nanostructures, assembled from crossover DNA nanorings, can potentially serve as DNA cages for the encapsulation of molecular cargo, similar to the recently described tetrahedral DNA assemblies.[16]

To obtain a mechanically stable rotaxane that exhibits the structure shown in Figure 4b, we ligated the branched spherical stoppers with the PX100 axle that contained the threaded macrocycle. The assembly was again monitored by agarose gel electrophoresis (Figure 4e). A threading efficiency of about 50% is evident from the ratio of the bands corresponding to the pseudorotaxane and the dumbbell structure (Figure 4e, lane 4). Upon addition of the two ROs, the mechanically stable rotaxane is formed (lane 5).

Figure 4f shows AFM images of the mechanically stable PX100–DNA rotaxane. These data reveal some remarkable properties of this novel class of DNA rotaxanes with a reinforced axle. First, the height profiles indicate that the spherical stoppers as well as the PX100 domain clearly stick out compared to both the macrocycle and the short double-stranded region at the ligation site. Of particular interest is the

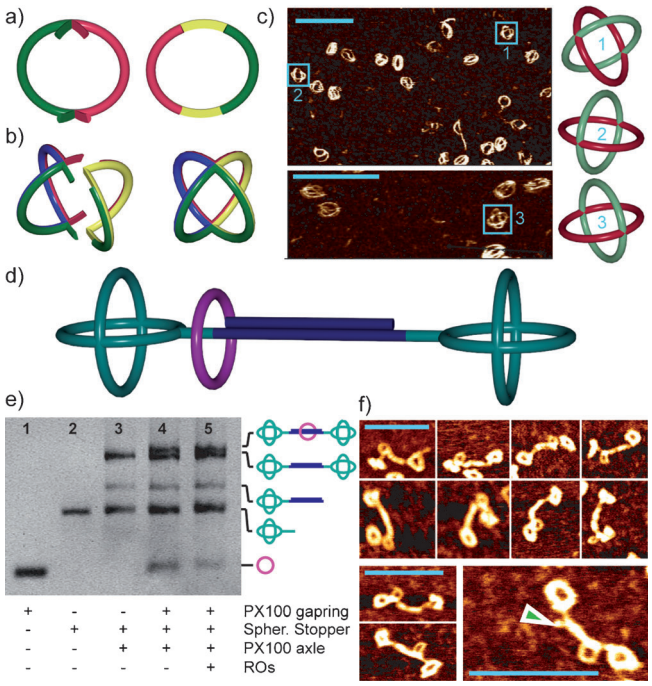

Figure 4. Assembly of the spherical DNA stoppers and the PX100 rotaxane. a) Simplified illustration of the intermediates present during the synthesis of the spherical stoppers: Ring B (left) containing four overhangs, ring C (right) containing two single-stranded gaps. b) Design of the Holliday junction (left) and depiction of the sphere containing four circular single strands (right). c) AFM images of the purified spheres (scale bar: 100 nm). d) Simplified image of the PX100 rotaxane containing spherical stoppers. In contrast to the pseudorotaxane that contains ring stoppers, this pseudorotaxane is transformed into a mechanically stable rotaxane after addition of the ROs. e) Agarose gel (2.2%) of the PX100 rotaxane synthesis. Lane 1: PX100 gap ring; lane 2: spherical stopper; lane 3: raw product of the dumbbell synthesis; lane 4: raw product of the pseudorotaxane synthesis with ca. 50% threading efficiency; lane 5: addition of the two ROs to the pseudorotaxane, transforming it into a mechanically stable rotaxane. f) AFM images of the purified rotaxane. The position of the macrocycle is no longer confined to the center (scale bar: 100 nm).

observation that in many of the scans shown in Figure 4 f, the DNA macrocycle appears to stay close to the stoppers, which proves that it has free room of motion. Moreover, the image depicted at the bottom right of Figure 4 f documents a structure in which the hairpin loop at the termini of the PX100 axle has taken an angular state (green arrow). AFM images of the purified PX100 axle confirm this observation (Supporting Information, Figure S4).

In summary, we have established a novel design strategy that allows the threading of a DNA macrocycle into a mechanically reinforced paranemic PX100 structure for the first time. The resulting DNA architecture can be ligated to spherical DNA stoppers, the improved assembly of which was shown as well. Addition of release oligodeoxynucleotides to the pseudorotaxane generated a stable DNA rotaxane that consists of an interlocked but fully mobile macrocycle and possesses a mechanically reinforced axle that, in contrast to the hitherto known DNA rotaxanes,[3] is almost nondistortable. This kind of interlocked DNA architectures should in principle be suitable for efficiently converting the motion of the macrocycle into mechanical energy and may find use in nanomechanics.

A number of biological processes are based on the efficient transmission of mechanical force. Prominent examples include muscle, motor, and transport proteins.[17] Thereby, the energy that is released through the binding of molecules or the hydrolysis of chemical bonds can lead to the generation of forces or mechanical work along a coordinate. In our further studies we seek to employ the DNA architectures reported herein for the transmission of forces in directed motion and to advance them in a way that enables them to perform mechanical work. Complex systems such as these require gradual advancements, like the approaches described herein for mechanical reinforcement and their integration into higher-order assemblies. In more general terms, these structures can be perceived as model systems that may be employed not only for emulating mechanical phenomena in biological systems but also for advancing our understanding of them.

Experimental Section

The DNA sequences used to assemble the PX100 axle were from Biolegio. All other sequences were from Metabion. All of the DNA sequences were provided HPLC-purified and contained a 5′-phosphate. See the Supporting Information for the sequences used in this study. Seeman buffer: 40 mM Tris, 20 mM AcOH, 12.5 mM $MgCl_2$, 2.5 mM EDTA. 1×DNA storage buffer: 10 mM Tris-HCl, 50 mM NaCl, 10 mM $MgCl_2$, pH 7.5.

HPLC purification: Weak anion-exchange (WAX) HPLC: column TSKgel DEAE-NPR 4.6 mm×35 mm (Tosoh); buffer A: 20 mM Tris-HCl, pH 9.0; buffer B: buffer A + 1M NaCl; gradient 40–65% B in 30 min. Following purification, the fractions were concentrated using Ultracel centrifugal filters (YM-30, YM-100, Millipore), washed with 2×DNA storage buffer, and stored in 100 μL DNA storage buffer.

Gel electrophoresis: Agarose gels were run in 0.5×TAE (Tris-acetate-EDTA) within 15–20 min at 120 V. Bands were visualized by ethidium bromide staining under UV light. The syntheses of the macrocycle and the stopper168 were performed as described.[3]

Assembly of DNA spheres: 1600 pmol of each DNA sequence (Supporting Information) for ring B und likewise for ring C were heated to 60°C in 1×ligase buffer (200 μL) (Fermentas) and cooled to 15°C at a 36°C h^{-1} rate. Ligase (4 μL, 20 U, Fermentas) was added and ligated at 15°C overnight. The two samples of ring B and ring C were combined, and again incubated with ligase (4 μL, 10 U) for 24 h at 15°. The raw product was purified by WAX-HPLC. The assembly of the spherical stoppers occurred by employing the same procedure, but by using the sequences ringSE a and ringSE b for ring C' instead of GE-5 (Supporting Information).

Assembly of the PX100 axle: The three DNA sequences HP-PX, AK1-PX, and AK2-PX (1000 pmol each) were heated to 95°C in Seeman buffer and cooled at a rate of 36°C h^{-1} to 15°C. The raw product was purified by WAX-HPLC, concentrated by using Ultracel centrifugal filters (YM-30, Millipore), and immediately rebuffered to Seeman buffer. The assembly was monitored by agarose gel electrophoresis (2.2%; Supporting Information).

Synthesis of the rotaxane: The PX100 axle (10 pmol, 1.0 equiv) and the PX100GR (2.0 equiv) were incubated in 1×ligase buffer containing additional $MgCl_2$ (25 mM final concentration) at 12°C overnight. The stopper molecules (ring stopper or spherical stopper, 2.5 equiv in each case) were added, and the samples were incubated in the presence of ligase (2 μL, 10 U) for 2 h at 12°C (final volume

100 μL). Subsequently, the longer-release oligo PXGR-RO (5 equiv) was added, followed 30 min later by the shorter PX-RO (10 equiv); ligation was continued for another 30 min. For the structural characterization by AFM, the ring-stopper-containing pseudorotaxane was purified by WAX-HPLC before addition of the ROs. The rotaxane containing the spherical stoppers was treated in the same way, but after addition of the ROs.

Atomic force microscopy (AFM): Nanowizard 3, JPK Instruments; measuring modes: HyperDrive in liquid (sphere); AC in air (rotaxane structures); substrate: mica with linear polyethylene imine as adhesive.

Received: April 12, 2012
Published online: May 31, 2012

Keywords: DNA nanorings · DNA nanotechnology · DNA rotaxanes · paranemic crossover · pseudorotaxanes

[1] a) V. V. Balzani, A. Credi, F. M. Raymo, J. F. Stoddart, *Angew. Chem.* **2000**, *112*, 3484 – 3530; *Angew. Chem. Int. Ed.* **2000**, *39*, 3348 – 3391; b) J. E. Beves, B. A. Blight, C. J. Campbell, D. A. Leigh, R. T. McBurney, *Angew. Chem.* **2011**, *123*, 9428 – 9499; *Angew. Chem. Int. Ed.* **2011**, *50*, 9260 – 9327; c) A. Coskun, M. Banaszak, R. D. Astumian, J. F. Stoddart, B. A. Grzybowski, *Chem. Soc. Rev.* **2012**, *41*, 19 – 30; d) E. R. Kay, D. A. Leigh, *Pure Appl. Chem.* **2008**, *80*, 17 – 29; e) E. R. Kay, D. A. Leigh, F. Zerbetto, *Angew. Chem.* **2007**, *119*, 72 – 196; *Angew. Chem. Int. Ed.* **2007**, *46*, 72 – 191; f) J. Sauvage, *Acc. Chem. Res.* **1998**, *31*, 611 – 619; g) C. A. Schalley, K. Beizai, F. Vögtle, *Acc. Chem. Res.* **2001**, *34*, 465 – 476.

[2] A. Moretto, I. Menegazzo, M. Crisma, E. J. Shotton, H. Nowell, S. Mammi, C. Toniolo, *Angew. Chem.* **2009**, *121*, 9148 – 9151; *Angew. Chem. Int. Ed.* **2009**, *48*, 8986 – 8989.

[3] D. Ackermann, T. L. Schmidt, J. S. Hannam, C. S. Purohit, A. Heckel, M. Famulok, *Nat. Nanotechnol.* **2010**, *5*, 436 – 442.

[4] P. Sa-Ardyen, A. V. Vologodskii, N. C. Seeman, *Biophys. J.* **2003**, *84*, 3829 – 3837.

[5] a) N. C. Seeman, *Annu. Rev. Biochem.* **2010**, *79*, 65 – 87; b) E. Stulz, G. Clever, M. Shionoya, C. Mao, *Chem. Soc. Rev.* **2011**, *40*, 5633 – 5635; c) A. V. Pinheiro, D. Han, W. M. Shih, H. Yan, *Nat. Nanotechnol.* **2011**, *6*, 763 – 772; d) a. D. Y. Zhang, G. Seelig, *Nat. Chem.* **2011**, *3*, 103 – 113; e) U. Feldkamp, C. M. Niemeyer, *Angew. Chem.* **2008**, *120*, 3933 – 3935; *Angew. Chem. Int. Ed.* **2008**, *47*, 3871 – 3873; f) Y. Krishnan, F. C. Simmel, *Angew. Chem.* **2011**, *123*, 3180 – 3215; *Angew. Chem. Int. Ed.* **2011**, *50*, 3124 – 3156.

[6] a) T. Wang, D. Schiffels, S. M. Cuesta, D. K. Fygenson, N. C. Seeman, *J. Am. Chem. Soc.* **2012**, *134*, 1606 – 1616; b) E. Stulz, *Chem. Eur. J.* **2012**, *18*, 4456 – 4469; c) N. Seeman, *Nature* **2003**, *421*, 427 – 431.

[7] a) E. Winfree, F. Liu, L. A. Wenzler, N. C. Seeman, *Nature* **1998**, *394*, 539 – 544; b) T. J. Fu, N. C. Seeman, *Biochemistry* **1993**, *32*, 3211 – 3220; c) X. Li, X. Yang, J. Qi, N. Seeman, *J. Am. Chem. Soc.* **1996**, *118*, 6131 – 6140; d) X. Yang, L. Wenzler, J. Qi, X. Li, N. Seeman, *J. Am. Chem. Soc.* **1998**, *120*, 9779 – 9786.

[8] a) C. H. Spink, L. Ding, Q. Yang, R. D. Sheardy, N. C. Seeman, *Biophys. J.* **2009**, *97*, 528 – 538; b) Z. Shen, H. Yan, T. Wang, N. C. Seeman, *J. Am. Chem. Soc.* **2004**, *126*, 1666 – 1674; c) X. Zhang, H. Yan, Z. Shen, N. C. Seeman, *J. Am. Chem. Soc.* **2002**, *124*, 12940 – 12941; d) K. A. Afonin, D. J. Cieply, N. B. Leontis, *J. Am. Chem. Soc.* **2008**, *130*, 93 – 102; e) P. K. Maiti, *Nucleic Acids Res.* **2004**, *32*, 6047 – 6056.

[9] a) H. Yan, X. Zhang, Z. Shen, N. C. Seeman, *Nature* **2002**, *415*, 62 – 65; b) P. E. Constantinou, T. Wang, J. Kopatsch, L. B. Israel, X. Zhang, B. Ding, W. B. Sherman, X. Wang, J. Zheng, R. Sha, N. C. Seeman, *Org. Biomol. Chem.* **2006**, *4*, 3414 – 3419.

[10] a) M. Santosh, P. K. Maiti, *Biophys. J.* **2011**, *101*, 1393 – 1402; b) P. K. Maiti, T. A. Pascal, N. Vaidehi, W. A. Goddard, *J. Nanosci. Nanotechnol.* **2007**, *7*, 1712 – 1720.

[11] a) P. Rothemund, *Nature* **2006**, *440*, 297 – 302; b) Y. Ke, N. V. Voigt, K. V. Gothelf, W. M. Shih, *J. Am. Chem. Soc.* **2012**, *134*, 1770 – 1774; c) Z. Zhao, Y. Liu, H. Yan, *Nano Lett.* **2011**, *11*, 2997 – 3002; d) T. Liedl, B. Högberg, J. Tytell, D. E. Ingber, W. M. Shih, *Nat. Nanotechnol.* **2010**, *5*, 520 – 524.

[12] For reviews, see: a) B. Saccà, C. M. Niemeyer, *Angew. Chem.* **2012**, *124*, 60 – 69; *Angew. Chem. Int. Ed.* **2012**, *51*, 58 – 66; b) F. C. Simmel, *Curr. Opin. Biotechnol.* **2012**, DOI: 10.1016/j.copbio.2011.1012.1024; c) W. M. Shih, C. Lin, *Curr. Opin. Struct. Biol.* **2010**, *20*, 276 – 282; d) T. Tørring, N. V. Voigt, J. Nangreave, H. Yan, K. V. Gothelf, *Chem. Soc. Rev.* **2011**, *40*, 5636 – 5646.

[13] a) G. Rasched, D. Ackermann, T. L. Schmidt, P. Broekmann, A. Heckel, M. Famulok, *Angew. Chem.* **2008**, *120*, 981 – 984; *Angew. Chem. Int. Ed.* **2008**, *47*, 967 – 970; b) T. L. Schmidt, C. K. Nandi, G. Rasched, P. P. Parui, B. Brutschy, M. Famulok, A. Heckel, *Angew. Chem.* **2007**, *119*, 4460 – 4462; *Angew. Chem. Int. Ed.* **2007**, *46*, 4382 – 4384; c) D. Ackermann, G. Rasched, S. Verma, T. L. Schmidt, A. Heckel, M. Famulok, *Chem. Commun.* **2010**, *46*, 4154 – 4156; d) G. Mayer, D. Ackermann, N. Kuhn, M. Famulok, *Angew. Chem.* **2008**, *120*, 985 – 987; *Angew. Chem. Int. Ed.* **2008**, *47*, 971 – 973.

[14] D. MacDonald, K. Herbert, X. Zhang, T. Polgruto, P. Lu, *J. Mol. Biol.* **2001**, *306*, 1081 – 1098.

[15] F. M. Raymo, J. F. Stoddart, *Pure Appl. Chem.* **1997**, *69*, 1987 – 1997.

[16] a) C. M. Erben, R. P. Goodman, A. J. Turberfield, *Angew. Chem.* **2006**, *118*, 7574 – 7577; *Angew. Chem. Int. Ed.* **2006**, *45*, 7414 – 7417; b) A. S. Walsh, H. Yin, C. M. Erben, M. J. Wood, A. J. Turberfield, *ACS Nano* **2011**, *5*, 5427 – 5432.

[17] a) C. Bustamante, Y. R. Chemla, N. R. Forde, D. Izhaky, *Annu. Rev. Biochem.* **2004**, *73*, 705 – 748; b) H. Herrmann, H. Bär, L. Kreplak, S. V. Strelkov, U. Aebi, *Nat. Rev. Mol. Cell Biol.* **2007**, *8*, 562 – 573; c) J. D. Humphrey, *Proc. R. Soc. London Ser. A* **2003**, *459*, 3 – 46; d) A. Kis, S. Kasas, B. Babić, A. Kulik, W. Benoît, G. Briggs, C. Schönenberger, S. Catsicas, L. Forró, *Phys. Rev. Lett.* **2002**, *89*, 248101.

